Polymer 51 (2010) 2887–2896

Contents lists available at ScienceDirect

Polymer

journal homepage: www.elsevier.com/locate/polymer

Electrospinning fabrication of partially crystalline bisphenol A polycarbonate nanofibers: The effects of molecular motion and conformation in solutions

Chia-Chun Liao [a], Sheng-Shu Hou [a], Cheng-Chien Wang [b], Chuh-Yung Chen [a,*]

[a] Department of Chemical Engineering, National Cheng Kung University, 70101 Tainan, Taiwan
[b] Department of Chemical and Materials Engineering, Southern Taiwan University, 71005 Tainan, Taiwan

ARTICLE INFO

Article history:
Received 16 October 2009
Received in revised form
14 April 2010
Accepted 23 April 2010
Available online 29 April 2010

Keywords:
Bisphenol A polycarbonate (BPAPC)
Nanofibers
Electrospinning

ABSTRACT

Partially crystalline bisphenol A polycarbonate (BPAPC) nanofibers were successfully fabricated using a combination of a centrifugal field (1800 rpm) and an electrostatic field (25 kV). The BPAPC solution properties are key factors for adequately electrospinning the partially crystalline BPAPC nanofibers. The correlation times (τ_c) of methyl ($\tau_c = 9.3$ ns) and of benzene-ring ($\tau_c = 15.3$ and 15.8 ns) motions in the 14 wt.% BPAPC/THF solution were longer than in CH_2Cl_2 and $CHCl_3$, as determined by NMR. The distribution-peak maximum of the hydrodynamic radius of BPAPC in the 14 wt.% THF solution ($R_h = 15$ Å) was higher than in CH_2Cl_2 ($R_h = 9.2$ Å) and $CHCl_3$ ($R_h = 7.9$ Å), as evidenced by DLS data. We conclude that the BPAPC assumed a denser, more worm-like chain conformation in THF solvation.

1. Introduction

An important property of bisphenol A polycarbonate (BPAPC) is its high impact strength even at well below its glass-transition temperature (150 °C). BPAPC has been widely used as an engineering polymer due to its toughness, weather durability, and transparency. BPAPC is difficult to crystallize in the bulk state and is therefore generally used in the amorphous state. However, many researchers [1–9] have concluded that BPAPC can be transformed into a partially crystalline state using specific methods, which consequently alter its mechanical properties. For example, Takahashi et al. [2] used a vapor-grown carbon fiber (VGCF) with a magnetic field to induce BPAPC crystallization. Hu and Lesser [4] incorporated nano-scale clay into a BPAPC resin in the presence of supercritical carbon dioxide; using this approach, the induction time for crystallization was reduced, and the crystallization rate increased significantly. Laredo et al. [6] predicted that BPAPC crystallization would be enhanced if BPAPC were blended with poly (ϵ-caprolactone).

Although there are many methods for preparing partially crystalline BPAPC [1–9], these processes require specific conditions. Accordingly, the development of a method for preparing partially crystalline BPAPC materials without complicated procedures is currently a very active research field. Furthermore, recent developments in nanotechnology have allowed organic and inorganic materials to be fabricated at the sub-microscale and nanoscale. Electrospinning has emerged as a promising technique for fabricating high-performance polymer nanofibers [10–28]. Although BPAPC has been electrospun into nanofibers by many groups, no evidence to date has emerged to suggest that partially crystalline BPAPC nanofibers could be prepared by electrospinning [29–41]. It is known that transformation of a polymer solution into nanofibers through electrospinning is influenced by various parameters [10,17]. These parameters include solution properties, operational and ambient variables in the electrospinning process, among which the polymer conformation in the solution used for electrospinning may be a key factor in determining the ultimate molecular structure of the electrospun polymer nanofibers.

Solvent-induced BPAPC crystallization has been investigated using both liquid solvation and solvent vapor techniques, each of which offers various advantages [42–52], mainly with regard to the kinetics of crystallization. A number of studies [53–64] have used both theoretical and experimental methods to investigate the behavior of BPAPC at the molecular level. However, several questions concerning the structure and motion of BPAPC remain open, for example: (a) Most researchers have focused mainly on local chain conformation in the solid BPAPC as evidenced using NMR data. To date, the relationships between *trans-trans*- and *trans-cis*-conformers, molecular motion, and the conformation of BPAPC dissolved in different solvents and their implications for fabricating partially crystalline BPAPC are not well understood. (b) The effects of reversible and nonreversible heat flows on the populations of

* Corresponding author. Tel.: +886 6 2360468; fax: +886 6 2344496.
E-mail address: ccy7@ccmail.ncku.edu.tw (C.-Y. Chen).

0032-3861/$ – see front matter © 2010 Elsevier Ltd. All rights reserved.
doi:10.1016/j.polymer.2010.04.046

trans-trans- and *trans-cis*-conformers in the partially crystalline BPAPC remain unclear.

In this study, we report that partially crystalline BPAPC nanofibers can be obtained via a new electrospinning process, in which an additional centrifugal force is exerted on the extruded polymer nanofibers. Three solvents (CH_2Cl_2, $CHCl_3$, and THF) were used to prepare the polymer solutions for electrospinning and only with THF were we able to obtain partially crystalline BPAPC nanofibers. The results imply that the final morphology of the nanofibers is closely related to the molecular motion and polymer conformation in the solution state. Therefore, the conformation, dynamics, and aggregation behavior of BPAPC in the three solvents were investigated using Raman and NMR spectroscopy together with DLS analysis.

2. Experimental

2.1. Materials

BPAPC resin pellets ($M_w = 1.68 \times 10^5$ g/mol, $M_n = 1.34 \times 10^5$ g/mol, polydispersity index ~1.25) were supplied by Chi-Lin Technology Co., Ltd. Dichloromethane (CH_2Cl_2, Aldrich Co. Ltd.), chloroform ($CHCl_3$, Aldrich Co. Ltd.), and tetrahydrofuran (THF, Aldrich Co. Ltd.) were selected as carrier solvents for this study.

2.2. Solution preparation

The polymer and solvents were used as received without purification. To prepare electrospinning solutions with different weight-percent concentrations (as listed in Table 1), pre-weighed amounts of polymer and solvents were mixed for several hours until homogeneous solutions were obtained. To fabricate the BPAPC nanofibers, the optimal amounts of BPAPC in the different solvents were 10 (CH_2Cl_2), 12 ($CHCl_3$), and 14 (THF) wt.%.

2.3. Novel electrospinning setup and electrospinning conditions

The apparatus used for horizontal dynamic spinneret electrospinning consisted of a computer-controlled power supply (range: 1–60 kV), a syringe pump (range: 0.05–10 mL/h), a three-phase induction motor (1800 rpm), a polytetrafluoroethylene (PTFE) tube (outer diameter of approximately 6 cm), and a copper ring (inner diameter of approximately 40 cm), as shown in Fig. 1(a)–(d).

In order to prevent interference from ambient variables, the electrospinning experiments were performed at 25 °C under the relative humidity of 68%. The optimal parameters for producing the BPAPC nanofibers were found as following: flow rate = 0.25 mL/h, spinneret tip-to-collector distance = 20 cm, electrical field = 25 kV, and centrifugal field = 1800 rpm. The residual solvent of the nanofibers was removed in a vacuum oven at 25 °C. After the solvent was completely removed, the nanofibers were subjected to SEM and XRD analyses and sealed in the aluminum pan for the subsequent MDSC analysis.

2.4. Analysis

A viscosity meter (AND Vibro-Viscometer SV-10, range: 0.3–10,000 mPa s), a conductivity meter (Trans Instruments WalkLAB A Microcontroller with LSI Technology Automatic Temperature Compensation, range: 0.1 μS-100.0 mS), and a surface-tension meter (FACE surface tensiometer CBVP-A3) were used to measure the solution properties (listed in Table 1) at 25 °C and at 68% relative humidity.

Modulated differential-scanning calorimetry (MDSC) measurements were carried out using a TA Instruments Q2000 Modulated DSC instrument. Samples were heated from 25 °C to 300 °C at 5 °C/min, 100 s modulation, and 1.326 °C modulation-temperature amplitude. MDSC uses two simultaneous heating rates, namely, linear and sinusoidal. The MDSC sinusoidal heating rate allows for separation of the total DSC heat flow signal into two components: the reversible component includes heat capacity and accounts for most of the melting activity, while the nonreversible component includes enthalpy relaxation and thermoset curing. Infrared spectra were recorded on a Varian 2000 FT-IR instrument under standard operating conditions. Each spectrum was calculated as the average of 50 scans at a resolution of 4 cm^{-1}. We saw a conformationally sensitive in-plane aromatic group-stretching vibration at 1600 cm^{-1} [65]. This band contained clearly identifiable contributions from *trans-trans*- and *trans-cis*-conformers at approximately 1594 cm^{-1} and 1604 cm^{-1}, respectively. The spectra in the range of 1500–1700 cm^{-1} were then analyzed individually using a commercially available curve-fitting program that was specially adapted to evaluate spectroscopy data (PeakFit).

Structural information was obtained from Raman scattering spectroscopy using an Nd:YAG laser with a wavelength of 532 nm as the light source. NMR experiments were performed on a Bruker AVANCE-500 spectrometer at resonance frequencies of 125.75 MHz for ^{13}C and 500.10 MHz for ^{1}H, respectively. The ^{13}C NMR chemical shifts were externally referenced to tetramethylsilane (TMS). All ^{13}C T_1 relaxation times were measured using the inversion-recovery pulse sequence. Dichloromethane-d_2 (Aldrich Co. Ltd.), chloroform-d_1 (Aldrich Co. Ltd.), and tetrahydrofuran-d_8 (Aldrich Co. Ltd.) were used as solvents in the NMR experiments. Requisite amounts of polymer and solvents were mixed for several hours until homogeneous solutions were obtained.

DLS measurements were carried out using an ALV/CGS-3 light-scattering spectrometer equipped with an ALV/LSE-5003 multiple-τ digital correlator. A JDS-Uniphase solid-state He–Ne laser with an output power of ~22 mW and operating wavelength of 632.8 nm was used as the light source. DLS is a highly effective tool for observing the dynamic behavior of polymer chains in solution given different length and time scales. With this technique, increases of hydrodynamic volume in the gelation region may be measured and sol–gel transitions can be readily identified [66].

Table 1
Physical properties of BPAPC dissolved in CH_2Cl_2, $CHCl_3$, and THF.

Solvent[a]	Weight Percent (wt.%)	Viscosity (cP)	Surface Tension (mN/m)	Operation Variables			
				Flow rate (mL/hr)	Spinneret tip-to-collector distance (cm)	Electrostatic field (kV)	Centrifugal field (rpm)
BPAPC **CH_2Cl_2** ($\epsilon = 9.1$)	10	37.3	28.4				
$CHCl_3$ ($\epsilon = 4.7$)	12	141.0	29.5	0.25	20	25	1800
THF ($\epsilon = 7.5$)	14	48.1	28.2				

[a] ϵ: permittivity.

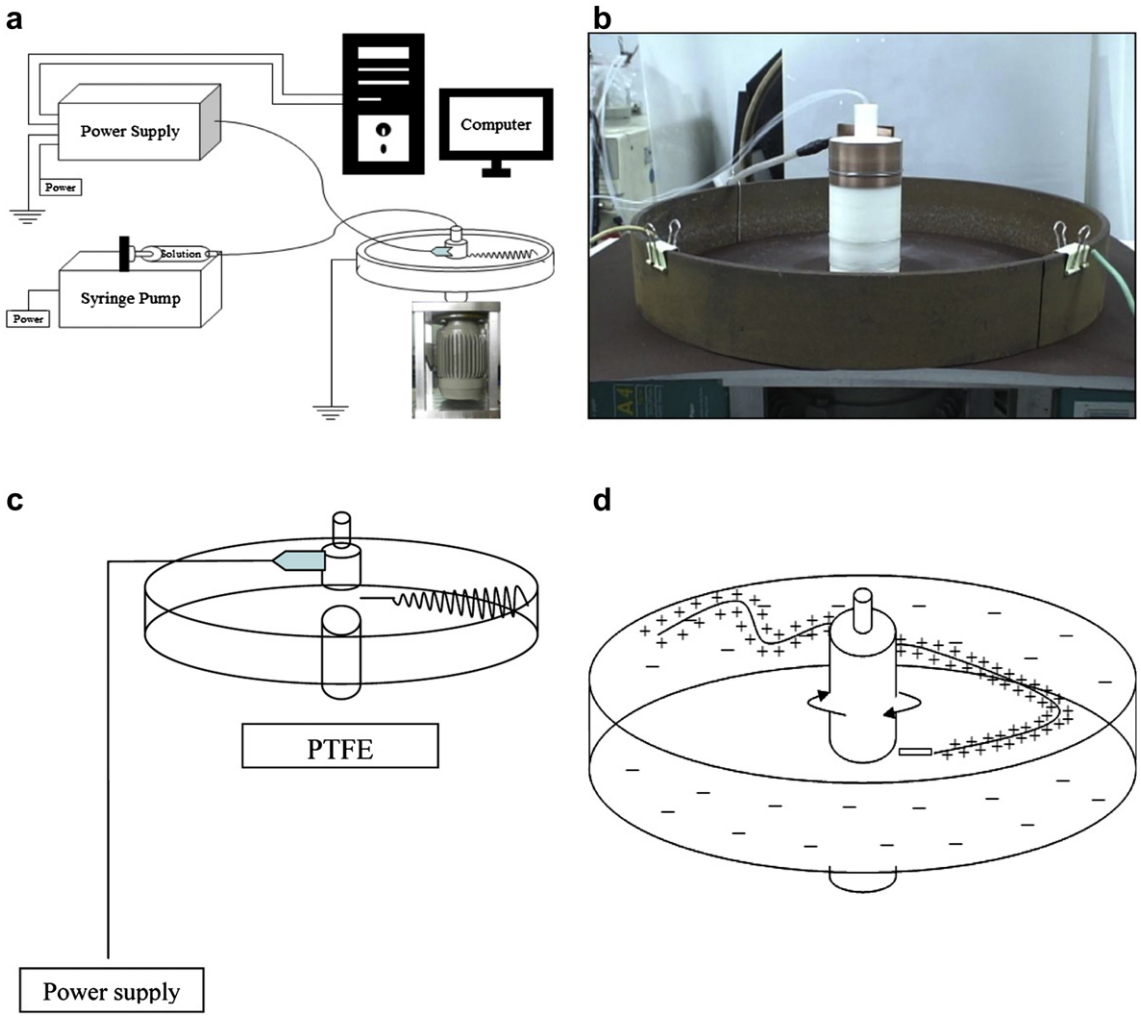

Fig. 1. Novel electrospinning technique for preparing partially crystalline BPAPC nanofibers; (a) Schematic illustration of the apparatus; (b) photograph of apparatus, (c) static motion of electrospinning, and (d) dynamic motion of electrospinning.

3. Results and discussion

3.1. Electrospinning conditions for the BPAPC nanofibers

Eight different solvents (chlorobenzene (C_6H_5Cl), chloroform ($CHCl_3$), dichloromethane (CH_2Cl_2), tetrahydrofuran (THF), 1,2-dichloroethane ($C_2H_4Cl_2$), 1,1,2,2-tetrachloroethane ($C_2H_2Cl_4$), 1,1,2,2-tetrachloroethylene (C_2Cl_4), *N*, *N*-dimethylformamide (DMF)) were initially selected attempting to prepare the BPAPC nanofibers. However, the high-quality BPAPC nanofibers could be produced only by using the BPAPC/CH_2Cl_2, BPAPC/$CHCl_3$, and BPAPC/THF solutions.

Furthermore, three different concentrations of polymer solution (10, 12, 14 wt.% for each solvent) were used for electrospinning. We found that uniform BPAPC nanofibers could be obtained by using 10 wt.% BPAPC/CH_2Cl_2, 12 wt.% BPAPC/$CHCl_3$, and 14 wt.% BPAPC/THF solutions, respectively. The uniform BPAPC nanofibers are uniaxially oriented without forming beaded nanofibers. The optimal parameters for producing the BPAPC nanofibers were found to be as follows: flow rate = 0.25 mL/h, spinneret tip-to-collector distance = 20 cm, electrical field = 25 kV, and centrifugal field = 1800 rpm. The BPAPC nanofibers obtained using THF as the solvent are partially crystalline. Nevertheless, the BPAPC nanofibers from the 10 wt.% BPAPC/CH_2Cl_2 and 12 wt.% BPAPC/$CHCl_3$ solutions are completely amorphous.

It should be noted that by means of the conventional electrospinning process and using THF as the solvent, the resulting BPAPC nanofibers are amorphous. Therefore, in addition to the solvent effect, the centrifugal force acting on the extruded fibers is also a key factor for producing the partially crystalline BPAPC nanofibers. The centrifugal field (1800 rpm) can effectively remove the perturbation phenomena, including the bending instability, during the electrospinning process. Moreover, the electrospun BPAPC nanofibers are uniaxially aligned in the presence of the centrifugal field. The strong stretching force from the centrifugal field, coupled with the preferred polymer conformation in the solution, probably can promote crystallization of the BPAPC fibers.

3.2. Crystallinity of the BPAPC nanofibers

As shown in the SEM images (Fig. 2(a)–(l)), most of the nanofibers were uniaxially aligned and exhibited favorable aspect ratios, superior to those produced by other fabrication processes [29–41]. The diameters of the BPAPC nanofibers prepared from the BPAPC in the CH_2Cl_2, $CHCl_3$, and THF solutions were approximately 1536; 967; and 221 nm, respectively. The diameter of the BPAPC nanofibers prepared from BPAPC in the THF solution was only 1/7 to 1/5 of that from the CH_2Cl_2 and $CHCl_3$ solutions. When examined under high magnification (Fig. 2(d)), the surfaces of the BPAPC nanofibers

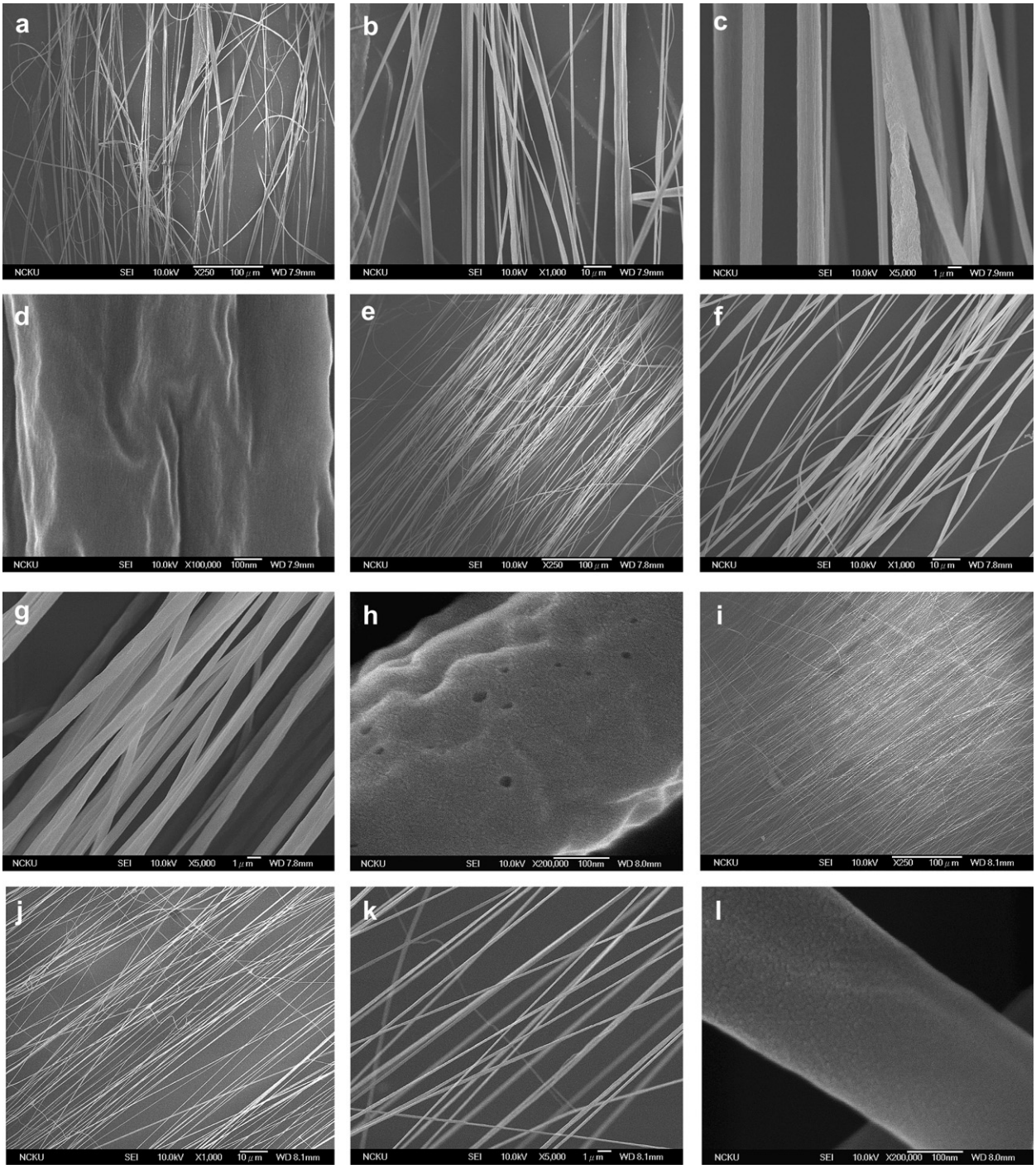

Fig. 2. FE-SEM images of uniaxially aligned BPAPC nanofibers. (a)–(d) BPAPC nanofibers prepared from BPAPC/CH_2Cl_2 solution, (e)–(h) BPAPC nanofibers prepared from BPAPC/$CHCl_3$ solution, and (i)–(l) BPAPC nanofibers prepared from BPAPC/THF solution at 25 kV and 1800 rpm. (The average diameter displayed in each sample was calculated by averaging over 30 fibers).

exhibited irregular puckers and wrinkles. In Fig. 2(h) and (l), the surfaces of the BPAPC nanofibers clearly exhibit irregular notches. The formation of puckers and notches might result from strong stretching on account of the combined electrostatic and centrifugal fields, together with rapid evaporation of the solvent.

MDSC was used to confirm the extent of crystallinity of the BPAPC nanofibers and to calculate the reversible heat flow ratio. In Fig. 3(a) and (b), the MDSC thermogram and deconvolution curves confirm that total, reversible, and nonreversible heat flow data were not correlated with melting behavior. As shown in Fig. 3(c), the proportions of reversible and nonreversible heat flows in the BPAPC nanofibers prepared by electrospinning were 75% (7.18 J/g) and 25% (2.33 J/g), respectively. The degree of crystallinity within the BPAPC nanofibers was approximately 6.5%. For comparison, the proportions of reversible and nonreversible heat flows in the THF-casting BPAPC film (Fig. 3(d)) prepared without electrospinning were 47% (2.64 J/g) and 53% (2.96 J/g), respectively. The degree of crystallinity of the THF-casting BPAPC film was approximately 2.4%.

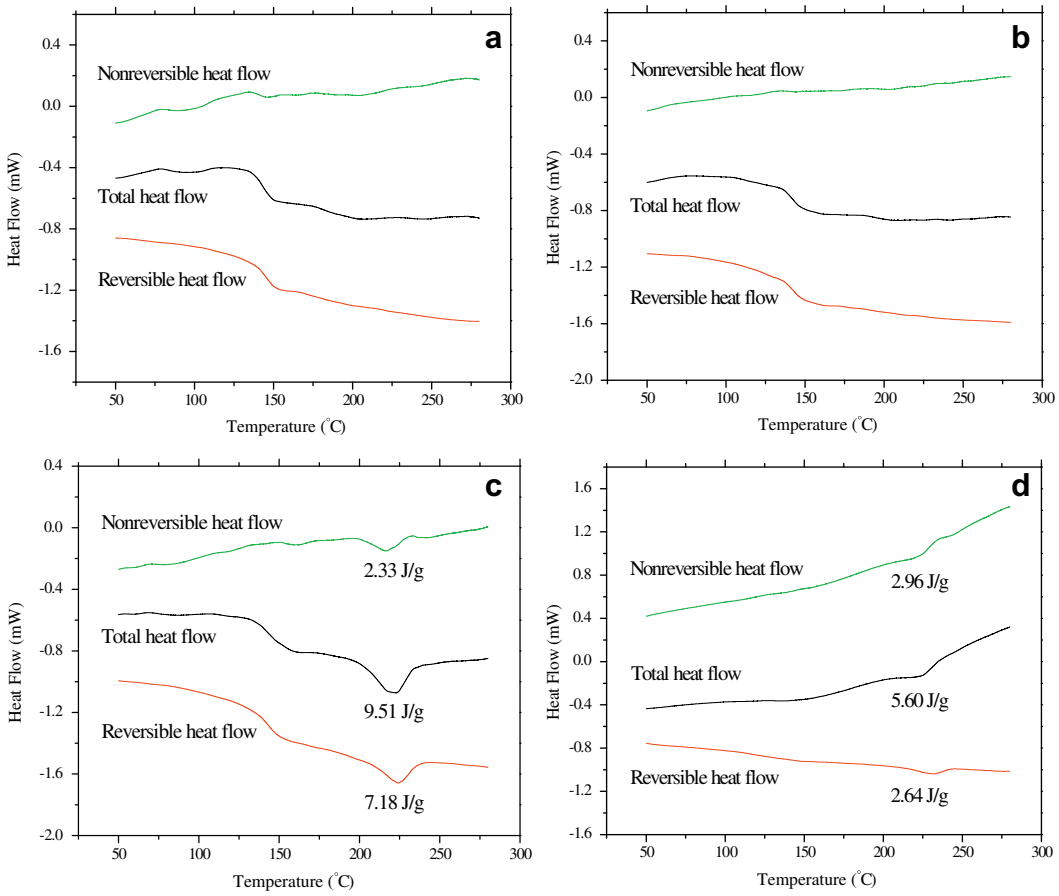

Fig. 3. The first-heating DSC curve of BPAPC nanofibers and membrane from 25 °C to 300 °C at 5 °C/min. (a) BPAPC nanofibers from BPAPC/CH_2Cl_2 solution with electrospinning, (b) BPAPC nanofibers from BPAPC/$CHCl_3$ solution with electrospinning, (c) BPAPC nanofibers from BPAPC/THF solution with electrospinning, and (d) BPAPC membrane from BPAPC/THF solution without electrospinning.

The electrospinning process can effectively decrease the degree of enthalpy relaxation and increase the BPAPC crystallinity to fabricate partially crystalline BPAPC nanofibers. The nanofibers that were prepared from the BPAPC in the CH_2Cl_2 or $CHCl_3$ solutions failed to exhibit any crystalline features. However, the BPAPC nanofibers prepared from the BPAPC/THF solution did exhibit crystalline features. Similarly, the BPAPC film exhibited crystalline features. In particular, Fig. 3(c) and (d) reveal that the proportion of nonreversible heat flow (enthalpic recovery or thermoset cure) for the BPAPC film without electrospinning was larger than for the BPAPC nanofibers that were produced using electrospinning.

The degree of crystallinity for the BPAPC nanofibers depends on the ratio of *trans-trans*-conformers, a metric that can be determined by FT-IR spectroscopy. Two idealized conformations were found that are consistent with existing fiber data on crystalline BPAPC [55]. The spectral band at 1600 cm^{-1} for in-plane aromatic-group-stretching vibrations is conformationally sensitive, containing clearly identifiable contributions from *trans-trans*- and *trans-cis*-conformers at approximately 1594 cm^{-1} and 1604 cm^{-1}, respectively [65]. In this study, all the spectra were put through a Lorentzian amplifier and curve-fitted using fixed peak positions to determine the areas under the peaks, as shown in Fig. 4(a)–(d). The ratios of the *trans-trans*- and *trans-cis*-conformers were calculated using the equation proposed by Lu et al. [67]. In Fig. 4(a), the percentages of *trans-trans* and *trans-cis* conformers in the BPAPC nanofibers prepared from the BPAPC/CH_2Cl_2 solution were 49% (1593 cm^{-1}) and 51% (1597 cm^{-1}), respectively. The percentages of *trans-trans*- and *trans-cis*-conformers in the BPAPC nanofibers prepared from the BPAPC/$CHCl_3$ solution were 53% (1593 cm^{-1}) and 47% (1599 cm^{-1}), respectively, as shown in Fig. 4(b). In Fig. 4(c), the percentages of *trans-trans*- and *trans-cis*-conformers in the BPAPC nanofibers prepared from the BPAPC/THF solution were 65% (1593 cm^{-1}) and 35% (1601 cm^{-1}), respectively. The percentages of *trans-trans*- and *trans-cis*-conformers in the BPAPC film were 45% (1592 cm^{-1}) and 55% (1601 cm^{-1}), respectively, as shown in Fig. 4(d). Fig. 4(c) illustrates how the fraction of *trans-trans*-conformers in BPAPC nanofibers prepared using electrospinning was higher than in the other fibers. Moreover, the changes in *trans-trans*- and *trans-cis*-conformers were not the sole factor of relevance to enthalpy relaxation. The diffusion of *trans-cis*-conformers along a chain may have contributed to enthalpy relaxation via a modification of interchain interactions [54]. Thus, the enthalpy relaxation was decreased substantially with the increasing fraction of *trans-trans*-conformers via the electrospinning process. MDSC and IR results revealed that the proportion of *trans-cis*-conformers in the partially crystalline BPAPC was consequently decreased on account of the electrospinning process.

The aforementioned results suggest that crystalline BPAPC nanofibers may only have been produced from the BPAPC/THF solution. In contrast, the BPAPC nanofibers that were fabricated from the BPAPC/CH_2Cl_2 and BPAPC/$CHCl_3$ solutions exhibited no crystalline features. In addition, the degree of crystallinity for the BPAPC nanofibers was strongly associated with the content of *trans-trans*-conformers of the polymer [64]. These facts suggest

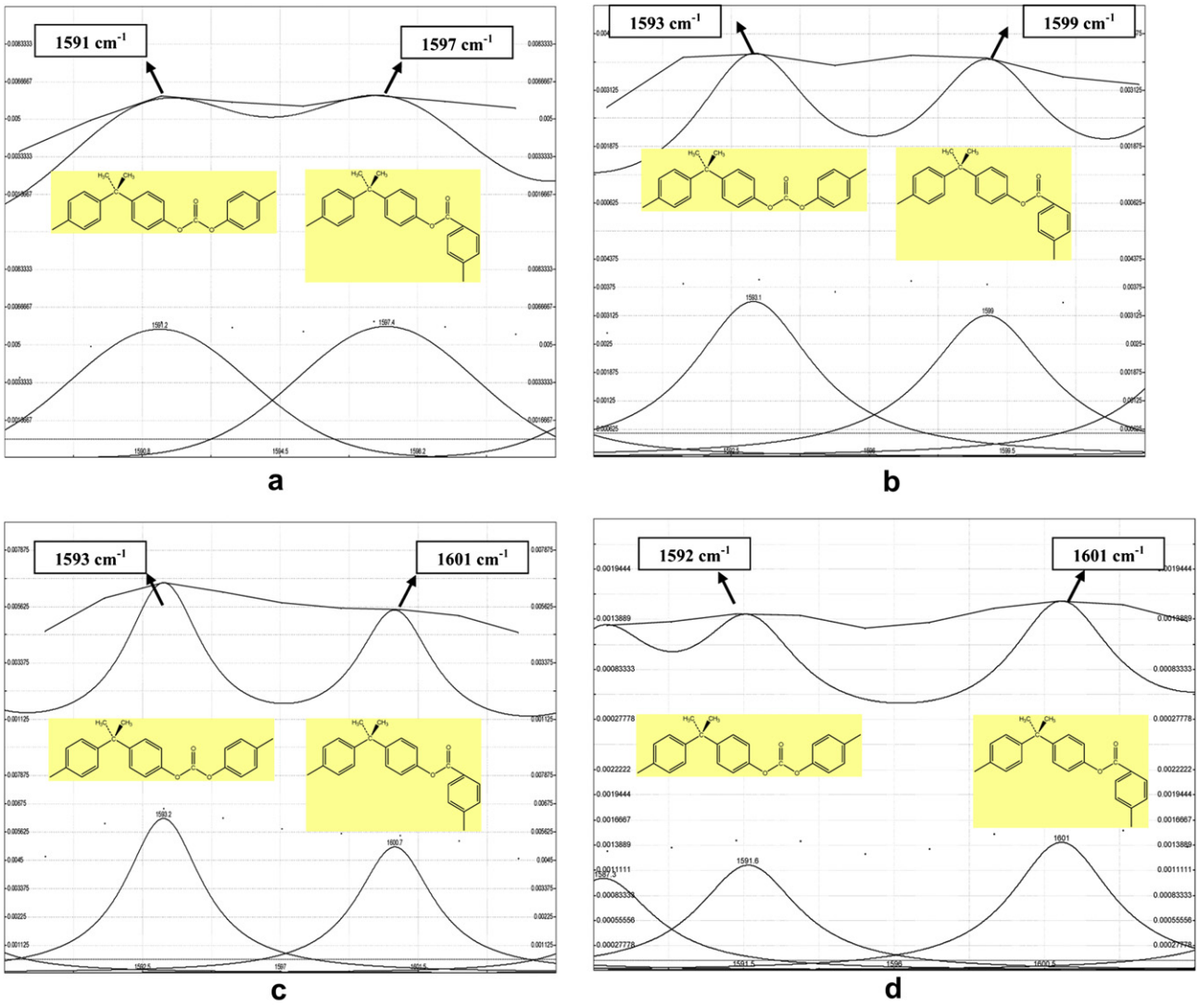

Fig. 4. Curve fitting of the IR spectra in the region between 1590 and 1605 cm^{-1}. The dotted spectrum is the original band contour. The solid spectrum is the curve-fitted band contour. (a) BPAPC nanofibers from BPAPC/CH_2Cl_2 solution with electrospinning, (b) BPAPC nanofibers from BPAPC/$CHCl_3$ solution with electrospinning, (c) BPAPC nanofibers from BPAPC/THF solution with electrospinning, and (d) BPAPC membrane from BPAPC/THF solution without electrospinning.

that increasing the *trans-trans*-conformers fraction of BPAPC in the solution state would favor the formation of crystalline BPAPC nanofibers by electrospinning. Furthermore, the fraction of *trans-trans*-conformers in the solution state has been found to vary with molecular motion [47,50]. In order to understand why the solvent is the most crucial factor in determining the final morphology of BPAPC nanofibers, we applied Raman, NMR, and DLS techniques to study the molecular motion and conformation of BPAPC in the different solvents.

3.3. Conformational analysis of BPAPC using Raman spectroscopy

To obtain further insight into the conformational behavior of $C_{carbonate}$—O—$C_{phenylene}$ moiety, the BPAPC solutions in CH_2Cl_2 ($\epsilon = 9.1$), $CHCl_3$ ($\epsilon = 4.7$), and THF ($\epsilon = 7.5$) were characterized by their Raman spectra, as shown in Fig. 5(a). In the 12 wt.% BPAPC/$CHCl_3$ solution, a doublet at 1240 and 1220 cm^{-1} appears in the Raman spectrum (Fig. 5(b)). However, in both the 10 wt.% BPAPC/CH_2Cl_2 and the 14 wt.% BPAPC/THF solutions, a broad band at 1240 cm^{-1} appears in the Raman spectra. Dybal et al. [64] have suggested that the bands exhibit frequency shifts due to the changing permittivity of the solvent. Fig. 5(b) shows the intensity of the high-frequency component of the doublet gradually increasing with greater permittivity. The transition from the amorphous to the crystalline (a shift from 1220 to 1240 cm^{-1}) was due to $C_{carbonate}$—O—$C_{phenylene}$-stretching vibrations. In the 14 wt.% BPAPC/THF solution, the $C_{carbonate}$—O—$C_{phenylene}$-stretching vibrations at 1030 cm^{-1} were more significant than in CH_2Cl_2 or $CHCl_3$ (Fig. 5(c)). These band shifts and band splittings in the $C_{carbonate}$—O—$C_{phenylene}$ stretching behavior can be explained by strong resonance transition dipole-transition dipole (TD) interactions of the closely ordered carbonate groups in the crystalline cell [64]. The band at 765 cm^{-1} in the amorphous form was shifted to 738 cm^{-1} in the crystalline form (Fig. 5(d)). The characteristic crystalline bands at 738 cm^{-1} in the Raman spectra corresponding to the localized skeletal vibrations were probably related to the regular ordering along the chain [64]. If sufficiently long regular sequences are present in the specimen, frequency shifts can result due to the presence of *all-trans*- sequences, as in the case of polyethylene reported by Snyder [68]. These data indicate that BPAPC in the THF

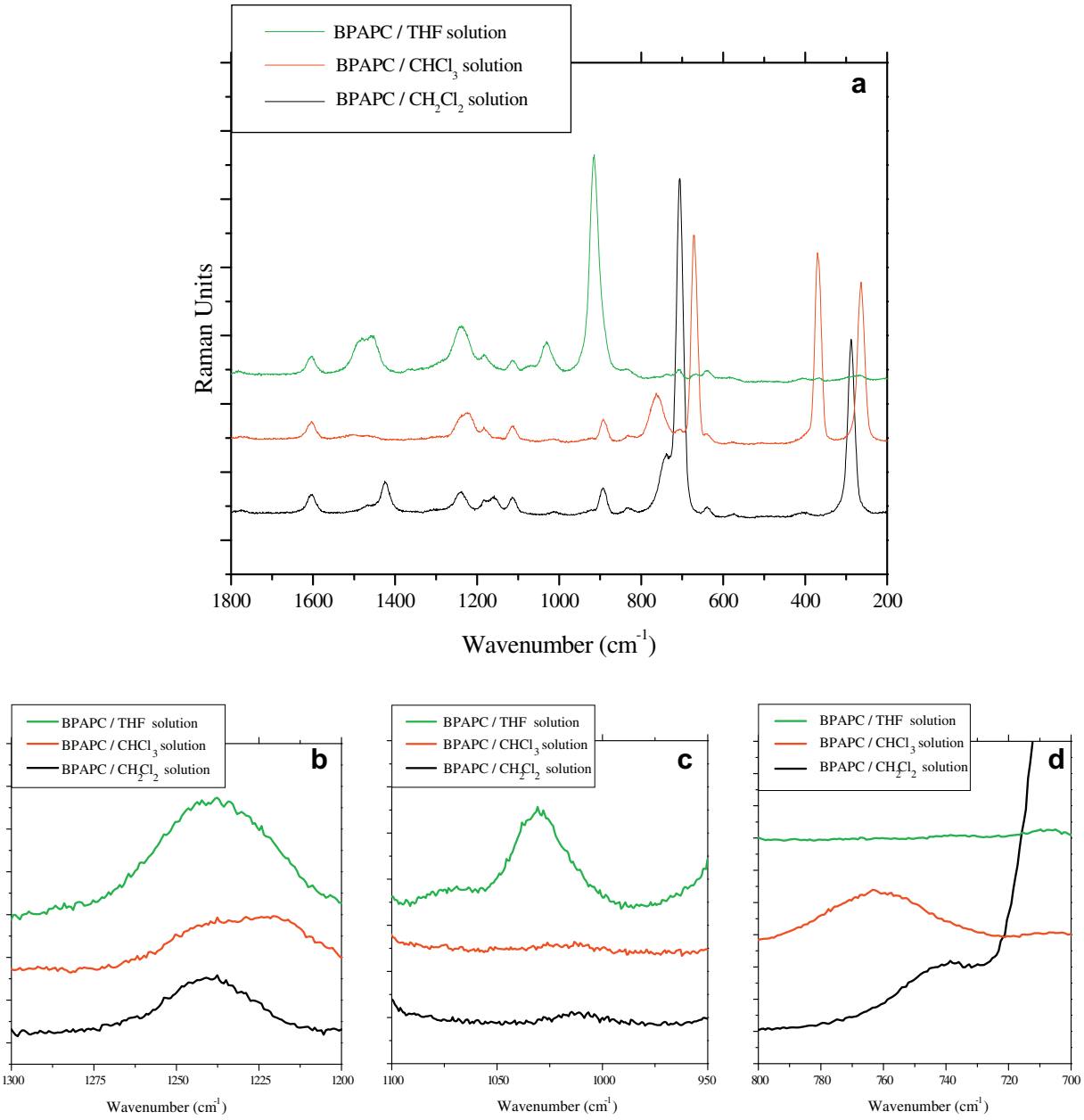

Fig. 5. Raman spectra of BPAPC: (a) BPAPC/CH_2Cl_2 ($\epsilon = 9.1$), $CHCl_3$ ($\epsilon = 4.7$), and THF ($\epsilon = 7.5$) solutions; (b) Bands corresponding to the $C_{carbonate}$–O–$C_{phenylene}$-stretching vibrations in the region of 1200–1300 cm^{-1}; (c) $C_{carbonate}$–O–$C_{phenylene}$-stretching vibrations in the region of 950–1100 cm^{-1}; (d) Amorphous and the crystalline forms in the region of 700–800 cm^{-1}.

solution favors *trans-trans*-conformation, but in CH_2Cl_2 or in $CHCl_3$, the *trans-cis*-conformation is favored. Additionally, the crystallinity was also substantially promoted with increasing fractions of *trans-trans*-conformers [64].

3.4. Molecular dynamics of BPAPC

Carbon-13 relaxation is commonly used to study the dynamics of polymers in polymer solutions, as the relaxation of protonated carbons can be attributed mainly to $^{13}C-^{1}H$ dipolar interactions from the attached protons. The relaxation rate of protonated ^{13}C can be interpreted using only the dipolar coupling. Furthermore, the ^{13}C spin-lattice relaxation time (T_1) and correlation time (τ_c) as computed from the simple dipolar-coupling model can be used to characterize gross changes in the segmental motions of polymers, as illustrated in Fig. 6. The ^{13}C spin-lattice relaxation rate is dominated by dipolar interactions between the carbon and its directly bonded protons, as described in Eq. (1):

$$\frac{1}{T_1^{DD}} = \frac{n}{10}\left(\frac{u_0}{4\pi}\right)^2 \frac{\gamma_C^2 \cdot \gamma_H^2 \cdot h^2}{\gamma^6}[J(\omega_H - \omega_C) + 3J(\omega_C) + 6J(\omega_H + \omega_C)] \quad (1)$$

where n is the number of directly attached protons, μ_0 is the vacuum magnetic permeability, γ_C and γ_H are the carbon and proton magnetogyric ratios, h is the Planck constant, γ is the internuclear distance, and ω_H and ω_C are the proton and carbon

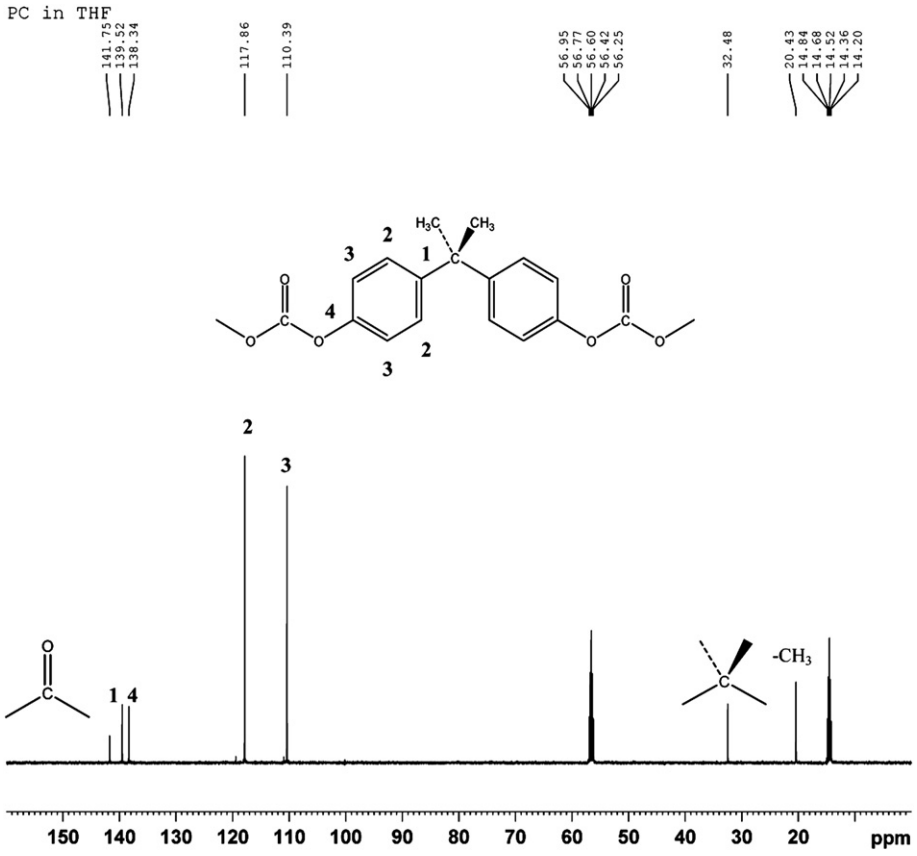

Fig. 6. Experimental dipolar patterns for a methyl carbon and an aromatic C–H pair at resonance frequencies of 125.75 MHz for ^{13}C and 500.10 MHz for ^{1}H for the 14 wt.% BPAPC in THF solution.

frequencies, respectively. The distance between the carbon and protons is 1.08 Å for the methyl carbon and 1.09 Å for the aromatic carbon. The spectral density function, $J(\omega)$, based on the isotropic rotation model, was used to calculate the rotational correlation time (τ_c).

Table 2 lists the τ_c values of the methyl and tertiary phenyl carbons of BPAPC in CH_2Cl_2-d_2, $CHCl_3$-d_1, and THF-d_8, respectively. We found that BPAPC in THF had the largest τ_c. A short τ_c is associated with rapid molecular motion and a long τ_c with restricted mobility [69]. The velocity of the horizontal flip of the methyl and benzene ring of the BPAPC in THF-d_8 was the slowest.

3.5. Dynamic behavior of polymer solution as revealed by DLS data

Fig. 7(a)–(c) show the normalized intensity-correlation function and the normalized distribution function as revealed by dynamic light scattering for the BPAPC in CH_2Cl_2, $CHCl_3$, and THF at 25 °C. In BPAPC nanofibers prepared from THF the crystallization is more pronounced, probably caused by the low solubility of the BPAPC in THF, in comparison with CH_2Cl_2 and $CHCl_3$. Here, we only discussed the nano-scale hydrodynamic radii (R_h). As shown in Fig. 7(a), the 10 wt.% BPAPC/CH_2Cl_2 solution yielded three peaks, indicating the R_h of 35 nm, 9.2 Å, and 0.2 Å. In Fig. 7(b), the 12 wt.% BPAPC/$CHCl_3$ solution featured two peaks at R_h of 67 nm and 7.9 Å. Fig. 7(c) shows the R_h in the 14 wt.% BPAPC/THF solution; of note, the correlation function is shifted to longer times along the relaxation–time axis; the R_h exhibits three peaks at 33 nm, 1.5 nm, and ~0.7 Å.

The second virial coefficient, A_2, and the statistical radius, $<S_2>^{1/2}$, obtained by static dynamic scattering, decreased significantly in the dilute BPAPC/THF solution [70]. From this, we could calculate the dimensionless quantity $A_2M_w/[\eta]$ as a function of $[\eta]/[\eta]_\theta$ for the BPAPC in CH_2Cl_2, $CHCl_3$, and THF. We used the intrinsic viscosity, $[\eta]$ and the value of $[\eta]$ at the theta condition, $[\eta]_\theta$, as reported by Berry et al. [71]. The interpenetration function, Ψ, as defined by $A_2M_w^2/(4\pi^{3/2}N_A<S_2>^{3/2})$ for flexible chains [72] was then calculated to be 0.19 for $CHCl_3$ and 0.17 for THF. The $A_2M_w/[\eta]$ and Ψ values suggest that the BPAPC chains in THF may not be completely flexible but are rather probably somewhat stiff or rigid [70,73]. It is known that flexible chains have smaller excluded-volume effects than stiff chains [74]. At a higher concentration, the influences due to interchain excluded-volume effects become more significant. Our experiment demonstrated that the attractive interaction between the

Table 2
Spin-lattice correlation time for a methyl carbon and an aromatic C–H pair for BPAPC dissolved in CH_2Cl_2, $CHCl_3$, and THF.

	Correlation time (τ_c)		
	Methyl	No. 2 position of phenyl ring	No. 3 position of phenyl ring
BPAPC/CH_2Cl_2 solution[a]	8.5 ns	13.1 ns	13.4 ns
BPAPC/$CHCl_3$ solution[b]	7.8 ns	10.2 ns	10.7 ns
BPAPC/THF solution[c]	9.3 ns	15.3 ns	15.8 ns

[a] The BPAPC content is 10 wt.%.
[b] The BPAPC content is 12 wt.%.
[c] The BPAPC content is 14 wt.%.

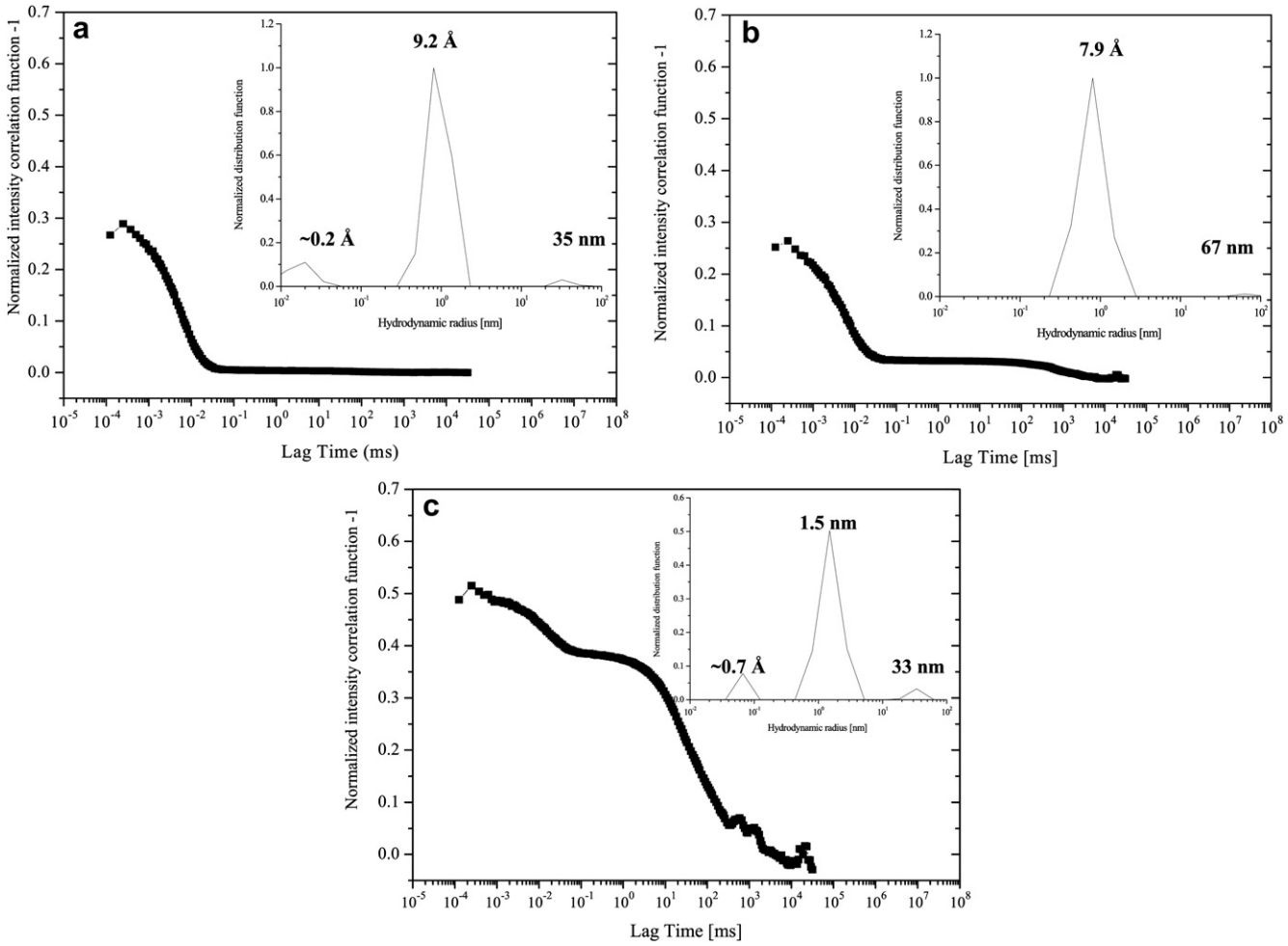

Fig. 7. Normalized intensity-correlation function, $g^2(t)$-1, of BPAPC in solution at comparable concentrations at $\theta = 90^\circ$ and at 25 °C: (a) BPAPC dissolved in CH_2Cl_2, (b) BPAPC dissolved in $CHCl_3$, and (c) BPAPC dissolved in THF. Inset: Corresponding normalized distribution function.

BPAPC and THF was very weak, barely inducing a smaller extension of the BPAPC chains.

We observed that the major R_h occurs at 9.2 Å in the case of CH_2Cl_2, which suggests that the internal relaxation modes of the networks can be divided into loose and tight conformations [75–78]. The loose conformation did not aggregate easily due to high affinity for the solvent [70]. The smallest R_h (~0.2 Å) may be attributed to flipping of the benzene ring in the aggregates. The BPAPC in $CHCl_3$ exhibited only the largest and major R_h. Since the free motion of benzene-ring flipping and the free translational diffusion of the individual chains are not affected by interchain aggregation, the smallest R_h did not exhibit any remarkable change. However, the major R_h of the BPAPC in $CHCl_3$ was smaller than in CH_2Cl_2, because the intramolecular and interchain motions of the aggregates became more active. Conversely, the major R_h of the BPAPC in THF was larger than in the case of CH_2Cl_2 and $CHCl_3$ because the intramolecular and interchain motions in the aggregates became more restricted. Thus, we conclude that a denser and more worm-like conformation resulting from the large excluded-volume effect served to restrict the mobility of the methyl and benzene ring.

Our results suggest that the polymer–solvent interaction between BPAPC and THF was weaker than in the case of CH_2Cl_2 and $CHCl_3$. The BPAPC chains probably adopted more densely worm-like conformations (or a more compact internal structure) in the THF case [70]. By contrast, the BPAPC chains preferentially adopted a more extended worm-like conformation in CH_2Cl_2 and $CHCl_3$. Chain collapse and aggregation probably occurred when the BPAPC/THF solution became more concentrated [47], and the collapse and aggregation from a more densely worm-like conformation may have induced crystallization.

4. Conclusions

Partially crystalline BPAPC nanofibers were successfully fabricated through electrospinning in our laboratory. The crystallinity of the BPAPC nanofibers was observed to increase proportionally with the fraction of *trans-trans*-conformers as determined by MDSC and PeakFit. The BPAPC in THF solution was a key factor for adequately electrospinning the partially crystalline BPAPC nanofibers. The effects of solvent quality on the molecular motion and conformation of the BPAPC in solutions with CH_2Cl_2, $CHCl_3$, and THF were characterized by Raman and NMR spectroscopy and DLS. In the 14 wt.% BPAPC/THF solution, the molecular motion, as determined by NMR, and the conformation, as determined by DLS, were both shown to promote *trans-trans*-sequences, resulting in higher crystallinity in the electrospun fibers.

Acknowledgements

The authors would like to gratefully acknowledge the National Science Council of the Republic of China (NSC-98-2622-E-006-015-CC3) for their financial support.

References

[1] Bae WJ, Jo WH, Park YH. Macromol Res 2002;10(3):145–9.
[2] Takahashi T, Yonetake K, Koyama K, Kikuchi T. Macromol Rapid Commun 2003;24(13):763–7.
[3] Kalkar AK, Siesler HW, Pfeifer F, Wadekar SA. Polymer 2003;44(23):7251–64.
[4] Hu X, Lesser AJ. Polymer 2004;45(7):2333–40.
[5] Li C, Kong Q, Fan Q, Xia Y. Mater Lett 2005;59(7):773–8.
[6] Laredo E, Grimau M, Barriola P, Bello A, Müller AJ. Polymer 2005;46 (17):6532–42.
[7] Lee JK, Im JE, Park JH, Won HY, Lee KH. J Appl Polym Sci 2006;99(5):2220–5.
[8] Yin B, Zhao Y, Yang W, Pan M-M, Yang M-B. Polymer 2006;47(25):8237–40.
[9] Lu J, Huang R, Oh I-K. J Polym Sci Polym Phys Ed 2007;45(19):2715–28.
[10] Huanga Z-M, Zhang Y-Z, Kotaki M, Ramakrishna S. Compos Sci Technol 2003;63(15):2223–53.
[11] Dzenis Y. Science 2004;304(5679):1917–9.
[12] Chronakis IS. J Mater Process Tech 2005;167(2–3):283–93.
[13] Ramakrishna S, Fujihara K, Teo W-E, Yong T, Ma Z, Ramaseshan R. Mater Today 2006;9(3):40–50.
[14] Teo WE, Ramakrishna S. Nanotechnology 2006;17(14):89–106.
[15] Greiner A, Wendorff JH. Angew Chem Int Ed 2007;46(30):5670–703.
[16] Park S, Park K, Yoon H, Son J-G, Min T, Kim G- H. Polym Int 2007;56(11):1361–6.
[17] Reneker DH, Yarin AL. Polymer 2008;49(10):2387–425.
[18] Wang X, Zhang K, Zhu M, Yu H, Zhou Z, Chen Y, et al. Polymer 2008;49 (11):2755–61.
[19] Wong S-C, Baji A, Leng S. Polymer 2008;49(21):4713–22.
[20] Nie H, He A, Zheng J, Xu S, Li J, Han CC. Biomacromolecules 2008;9(5):1362–5.
[21] Chen H, Liu Z, Cebe P. Polymer 2009;50(3):872–80.
[22] Hellmann Ch, Belardi J, Dersch R, Greiner A, Wendorff JH, Bahnmueller S. Polymer 2009;50(5):1197–205.
[23] Gandhi M, Yang H, Shor L, Ko F. Polymer 2009;50(8):1918–24.
[24] Shah PN, Manthe RL, Lopina ST, Yun YH. Polymer 2009;50(10):2281–9.
[25] Zhou Z, Lai C, Zhang L, Qian Y, Hou H, Reneker DH, et al. Polymer 2009;50 (13):2999–3006.
[26] Desai K, Kit K, Li J, Davidson PM, Zivanovic S, Meyer H. Polymer 2009;50 (15):3661–9.
[27] Nie H, He A, Wu W, Zheng J, Xu S, Li J, et al. Polymer 2009;50(20):4926–34.
[28] Munir MM, Suryamas AB, Iskandar F, Okuyama K. Polymer 2009;50 (20):4935–43.
[29] Krishnappa VN, Desai K, Sung CJ. Mater Sci 2003;38(11):2357–65.
[30] Tsai PP, Chen WW, Roth JR. Inter Nonwoven J 2004;13(3):17–23.
[31] Viswanathamurthi P, Bhattarai N, Kim HY, Cha DI, Lee DR. Mater Lett 2004;58 (26):3368–72.
[32] Shawon J, Sung C. J Mater Sci 2004;39(14):4605–13.
[33] Kattamuri N, Sung C. NSTI-Nanotech 2004;3:425–8.
[34] Wei M, Lee J, Kang B, Mead J. Macromol Rapid Commun 2005;26 (14):1127–32.
[35] Meechaisue C, Dubin R, Supaphol P, Hoven VP, Kohn J. J Biomater Sci Polymer Ed 2006;17(9):1039–56.
[36] Wei M, Kang B, Sung C, Mead J. Macromol Mater Eng 2006;291(11):1307–14.
[37] Han X-J, Huang Z-M, He C-L, Liu L, Wu Q-S. Polym Composites 2006;27 (4):381–7.
[38] Welle A, Kröger M, Döring M, Niederer K, Pindel E, Chronakis IS. Biomaterials 2007;28(13):2211–9.
[39] Kim SJ, Nam YS, Rhee DM, Park H-S, Park WH. Eur Polym J 2007;43 (8):3146–52.
[40] Sihn S, Kim RY, Huh W, Lee K-H, Roy AK. Compos Sci Technol 2008;68 (3–4):673–83.
[41] Moon S-C, Farris RJ. Polym Eng Sci 2008;48(9):1848–54.
[42] Daniewska I, Dobkowski Z, Cz'ionkowska-Kohutnicka Z. J Appl Polym Sci 1986;31(8):2401–5.
[43] Durning CJ, Rebenfeld L, Russel WB, Weigmann HD. J Polym Sci Polym Phys Ed 1986;24(6):1321–40.
[44] Durning CJ, Rebenfeld L, Russel WB, Weigmann HD. J Polym Sci Polym Phys Ed 1986;24(6):1341–60.
[45] Harron HR, Pritchard RG, Cope BC, Goddard DT. Int J Electronics 1996;81 (4):485–9.
[46] Harron HR, Pritchard RG, Cope BC, Goddard DT. J Polym Sci Polym Phys Ed 1996;34(1):173–80.
[47] Park D, Hong J-W. Polym J 1997;29(12):970–4.
[48] Aharoni SM, Sanjeeva Murthy N. Inter J Polym Mater 1998;42(3–4):275–83.
[49] Hsu W-P. J Appl Polym Sci 2001;80(14):2842–50.
[50] van Aert HAM, Nelissen L, Lemstra PJ, Brunelle DJ. Polymer 2001;42 (5):1781–8.
[51] Stolarczyk JK, Grzywna ZJ, Koziol KKK. Polymer 2004;45(5):1525–32.
[52] Fan Z, Shu C, Yu Y, Zaporojtchenko V, Faupel F. Polym Eng Sci 2006;46 (6):729–34.
[53] Schaefer J, Stejskal EO, McKay RA, Thomas Dixon W. Macromolecules 1984;17 (8):1479–89.
[54] Jones AA. Macromolecules 1985;18(5):902–6.
[55] Perez S, Scaringe RP. Macromolecules 1987;20(1):68–77.
[56] Henrichs PM, Luss HR, Scaringe RP. Macromolecules 1989;22(6):2731–42.
[57] Henrichs PM, Nicely VA. Macromolecules 1990;23(12):3193–4.
[58] Henrichs PM, Nicely VA. Macromolecules 1991;24(9):2506–13.
[59] Hutnik M, Argon AS, Suter UW. Macromolecules 1991;24(22):5956–61.
[60] Iyer VS, Sehra JC, Ravindranath K, Sivara S. Macromolecules 1993;26 (5):1186–7.
[61] Klug CA, Zhu W, Tasaki K, Schaefer J. Macromolecules 1997;30(6):1734–40.
[62] Whitney DR, Yaris R. Macromolecules 1997;30(6):1741–51.
[63] Tomaselli M, Zehnder MM, Robyr P, Grob-Pisano C, Ernst RR, Suter UW. Macromolecules 1997;30(12):3579–83.
[64] Dybal J, Schmidt P, Baldrian J, Kratochvıl J. Macromolecules 1998;31 (19):6611–9.
[65] Heymans N, Rossum SV. J Mater Sci 2002;37(20):4273–7.
[66] Fang L, Brown W, Konak C. Macromolecules 1991;24(26):6839–42.
[67] Lu J, Wang Y, Shen D. Polym J 2000;32(7):610–5.
[68] Snyder RG. J Chem Phys 1967;47(4):1316–59.
[69] Mirau PA. A practical guide to understanding the NMR of polymers. Wiley-Interscience; 2005.
[70] Tsuji T, Norisuye T, Fujita H. Polym J 1975;7(5):558–69.
[71] Berry GC, Nomura H, Mayhan KG. J Polym Sci Polym Phys Ed 1967;5(1):1–21.
[72] Yamakawa H. Pure Appl Chem 1972;31(1–2):179–99.
[73] Sitaramaiah G. J Polym Sci Polym Chem Ed 1965;3(8):2743–57.
[74] Akashi K, Nakamura Y, Norisuye T. Polymer 1998;39(21):5209–13.
[75] Schmitz KS. An introduction to dynamic light scattering by macromolecules. Academic Press; 1990.
[76] Li YC, Chen KB, Chen HL, Hsu CS, Tsao CS, Chen JH, et al. Langmuir 2006;22 (26):11009–15.
[77] Li YC, Chen CY, Chang YX, Chuang PY, Chen JH, Chen HL, et al. Langmuir 2009;25(8):4668–77.
[78] Chen JH, Chang CS, Chang YX, Chen CY, Chen HL, Chen SA. Macromolecules 2009;42(4):1306–14.